

1. Identification and Significance of the Innovation

One of the key areas of study of NASA's Earth Science enterprise is the role played by clouds and aerosols in climate change (USGCRP 1995). The Earth Observing System (EOS) is a constellation of NASA satellites intended to monitor clouds, aerosols, oceans, landmasses and their effects on climate change over the next 10 to 20 years. The flagship, Terra, was launched in December 1999 (<http://terra.nasa.gov/>). Aura was launched in 2002, the first of a series of six 'A-Train' satellites, the last of which is scheduled to be deployed in 2006 (<http://radio.weblogs.com/0105910/2004/05/24.html>). However, satellite measurements of the size, shape and concentration of cloud and aerosol particles are determined by mathematical inversion of (passive and active) radiative signatures from distances of 700 km. Thus, in situ validation of retrieval algorithms used to determine cloud and aerosol properties is essential.

Research aircraft equipped with sensors to probe the microphysical properties of aerosols and clouds have been in use for over fifty years, but the duration of conventional aircraft is limited so that long-term measurements are not practical, and long-term, high-coverage measurements are needed to provide a statistical basis for comparing with satellite measurements. Small uninhabited aerial vehicles (UAVs) and tethered balloons, however, are now capable of making sustained, long-term (30 hr) measurements, so that data sets can be collected that provide much better statistical comparisons with results from satellite retrieval algorithms. In addition, several small UAVs and tethered balloons can be deployed simultaneously to improve spatial coverage of the measurements.

Lightweight, low-power cloud and aerosol sensors are needed for applications on small, relatively low-cost, long-duration UAVs and tethered balloons in order to validate satellite measurements.

2. Results of the Phase I Research

2.1 Overview

In Phase I, we investigated the feasibility of adapting three existing sensors commonly used on piloted research aircraft for use on small UAVs. The three technologies are

- a hot-wire liquid water content probe (e.g., SkyTech Nevzorov probe, Korolev et al. (1998)).
- a particle scattering spectrometer probe (e.g., Particle Measuring Systems (PMS) forward scattering spectrometer probe (FSSP), Knollenberg 1981; Droplet Measuring Technologies (DMT) Cloud and Aerosol Spectrometer (CAS), Baumgardner et al. (2002)), and
- a cloud particle imager (CPI), Lawson et al. (2001).

We evaluated each of these technologies, which in their current form factor are far too heavy and consume too much power, to determine those that could best be adapted for use on small UAVs.

The Aerosonde was chosen as the primary target UAV (Figure 1) because it is the most commonly used UAV for weather research (see <http://paos.colorado.edu>, www.aerosonde.com and Holland et al. 2001), it is relatively low-cost, has long (30 hr) duration, and in addition, Aerosonde Pty Ltd of Melbourne, Australia (hereafter called Aerosonde Corporation) has agreed to be a Phase II and Phase III partner with SPEC. Aerosonde Corporation will contribute significant technical support in Phase II and will provide production and marketing in Phase III. See Supporting Documents Section for more information on Aerosonde Corporation's participation in Phases II and III.

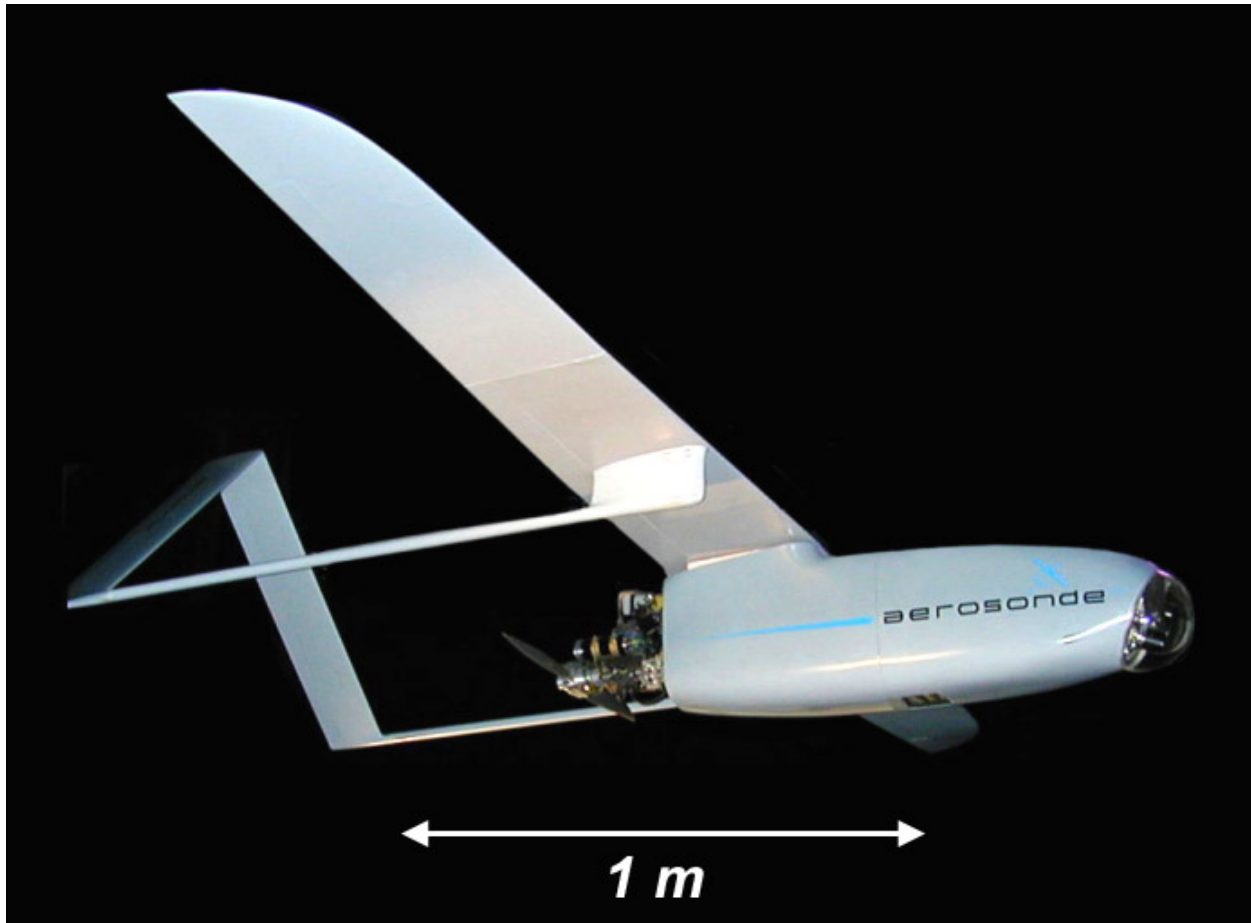


Figure 1. Photograph of the Aerosonde UAV selected as a target for feasibility studies in Phase I.

While it was deemed (marginally) technically feasible to generate sufficient electrical power to de-ice and heat a hot-wire sensor, it was considered to be too much of an investment for only one measurement, which is the mass concentration of liquid water, commonly called the liquid water content (LWC). As a result, investigations into development of a suitable hot-wire sensor were dismissed and emphasis was placed on the other two candidate technologies.

The other two technologies, an aerosol and cloud particle scattering probe and a cloud particle imager, are much more attractive in that they give considerably more information, including:

- cloud drop size distribution,
- aerosol size distribution,
- ice particle size distribution,
- high-resolution images of ice particles and water drops.

Derived parameters from the above measurements include (but are not limited to):

- cloud drop concentration
- mean Cloud drop size
- liquid water content
- ice particle concentration
- ice water content (IWC)
- ice particle shape and crystal habit
- cloud extinction
- cloud effective particle size
- cloud equivalent radar reflectivity
- aerosol size distribution

We determined that the scattering and imaging technologies could be combined into a single instrument that contributes minimally to aerodynamic drag, consumes little power, does not need to be deiced and weighs about 1.2 Kg. Figure 2 shows a Solidworks model of the new instrument, called a Micro-CPI, as it would be appear when installed on the Aerosonde.

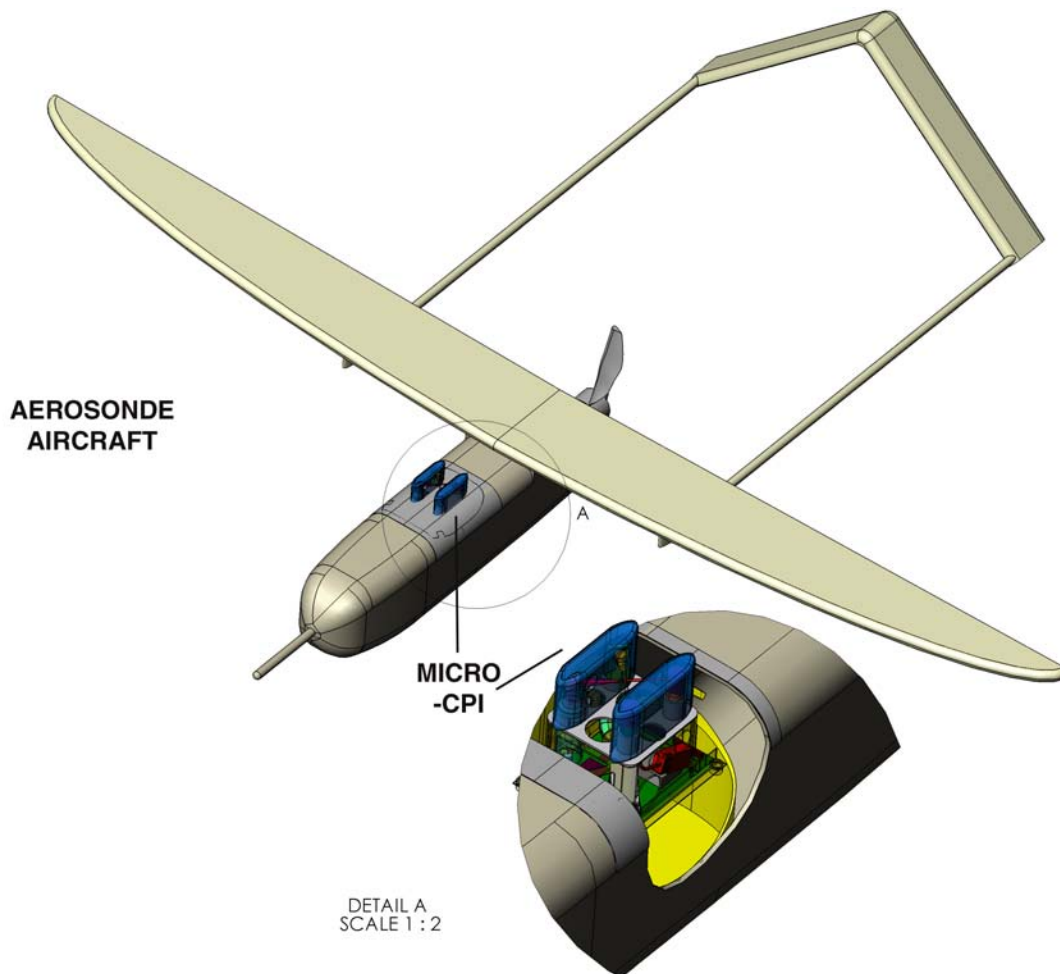


Figure 2. Solidworks model of the Micro-CPI as it will appear when installed on the Aerosonde.

SPEC worked closely with Aerosonde during Phase I to assure that the Micro-CPI will fit seamlessly into the UAV. Aerodynamics, aircraft center of gravity, power loading and sensitivity to vibration were all considered in the design of the Micro-CPI. Details of the design process and parameters are described in **Sections 2.2 – 2.11**. Aerosonde expects Phase III commercial sales of 10 to 20 Micro-CPIs per year initially and will make a significant contribution to the Phase II effort. Aerosonde has agreed to subcontract 640 hours in Phase II; 320 of these hours will be contributed by Aerosonde (see Budget and Aerosonde Letter of Cooperation). Aerosonde's home office is in Australia. However the company also has a facility at the NASA Wallops Island Research Center, and has agreed to make available and support a new Aerosonde Piccolo for flight tests of the Micro-CPI in Phase II.

The commercially available CPI, used on piloted aircraft, has a particle detection system (PDS) that identifies candidate cloud particles and triggers the imaging system. The Micro-CPI will use an innovative particle detection system, that in addition to detecting candidate particles, will simultaneously count and size particles, including aerosols, cloud drops and ice particles. The new PDS is called a forward scattering system (FSS) because it uses focused optics with forward scattered light and qualifying detectors, similar to the FSSP and CAS, to define particle depth of field and pulse height to determine particle size. Like the FSSP and CAS, the FSS particle sizing is based on the

assumption that particles have a spherical shape. The following subsections in **Section 2** describe in detail the design of the Micro-CPI.

2.2 Micro-CPI Imaging Optical System

Figure 3 shows a ray-trace of the imaging optical system for the Micro-CPI. The system is based on a Keplerian telescope operating at a finite conjugate ratio. Particles passing through the sample volume are imaged onto the CMOS camera array. A pulsed laser (not shown) is used to illuminate the particle as it passes through the sample volume. The laser pulse width is much shorter than the exposure time of the CMOS camera chip, thereby freezing the motion of a particle in flight.

The working distance for a lens system is the distance from the front of the first lens to the object plane. For this system the working distance is also equivalent to the focal length of Lens 1. The magnification for the optical system is determined by the ratio of the focal lengths of Lens 2 to Lens 1 and the total path length is twice the sum of the focal lengths of Lens 1 and Lens 2. The focal length of Lens 1 must be chosen based on the instrument layout in the Aerosonde. Lens 2 can then be selected to provide the necessary system magnification and balance the total path length limited by the instrument layout. In this case, Lens 1 is chosen to have a focal length of 35 mm and Lens 2 is chosen to have a focal length of 85 mm. The working distance for this system is then 35 mm. The system magnification is $-85/35 \sim -2.4X$. The negative sign implies the image is inverted. The total path length is $2 \times (85 + 35)$ or 240 mm. The CMOS array chip selected for the system is a Symagery VCA 1281 with 1024×1280 pixels that are $7 \mu\text{m} \times 7 \mu\text{m}$ each. The system resolution is $7 \mu\text{m} / 2.4X$ or approximately $2.92 \mu\text{m pixel}^{-1}$ in the sample volume. The sample volume dimensions are $2.92 \mu\text{m pixel}^{-1} \times (1024 \times 1280)$ pixels or $2.99 \text{ mm} \times 3.74 \text{ mm}$.

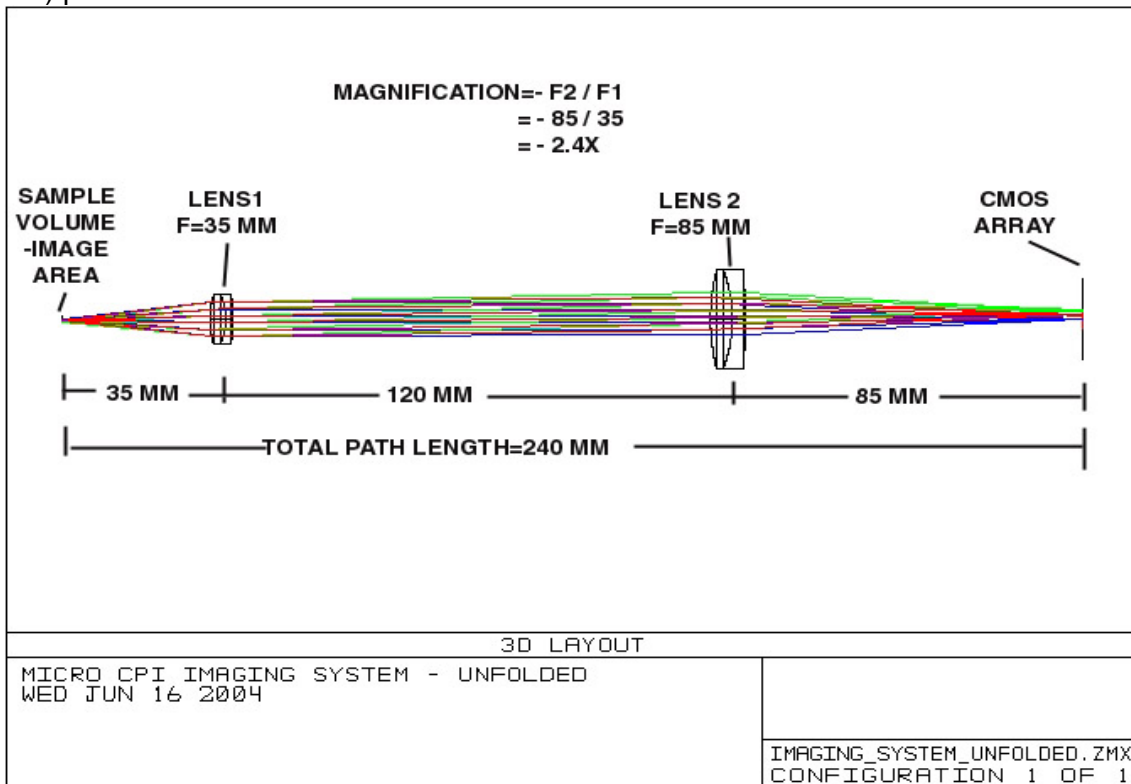


Figure 3. Zemax ray trace of Micro-CPI imaging optical system.

The imaging system design shown in **Figure 3** was prototyped in the laboratory. **Figure 4** is a photograph of the prototype imaging system. A Scorpion camera manufactured by Point Grey Research was purchased. The Scorpion camera uses the Symagery VCA 1281 CMOS chip. For the Micro-CPI instrument proposed in Phase II, the Scorpion camera will not be used, but the CMOS chip will be integrated into a custom designed circuit board. The imaging laser used in the prototype system is a CW diode laser operating at 680 nm. The laboratory system was used to capture images of glass beads and reticles on a slide. Since the objects are stationary, a pulsed laser is not required to freeze the motion of the objects.

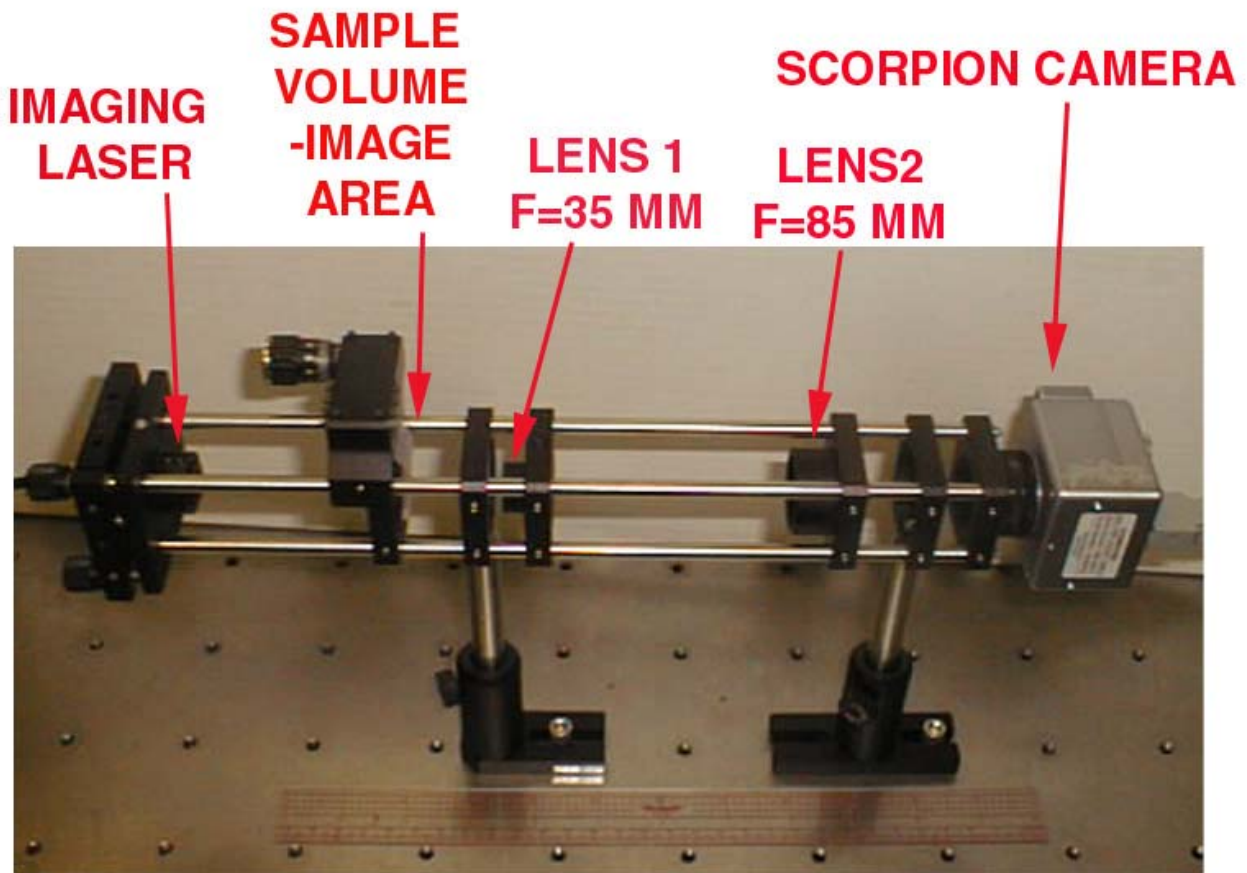


Figure 4. Photograph of prototype Micro-CPI imaging system using a Scorpion CMOS camera.

Images of various glass beads and reticles captured with the prototype imaging system are shown in **Figure 5**. The resolution for the prototype system is $2.87 \text{ } \mu\text{m pixel}^{-1}$. The resolution is calculated by counting the total number of pixels in a horizontal line shadowed by the 500 μm disc reticle. Particles are identified by the depth of the shadow created by the particle contrasted to the area around the particle. This resolution is sufficient to easily identify particles less than 10 microns in diameter, as shown in the top of **Figure 5**. The actual resolution is very close to the theoretical resolution of $2.92 \text{ } \mu\text{m pixel}^{-1}$. For comparison purposes, images of ice

crystals taken with the commercially available CPI, which has 2.3 μm pixel resolution, are shown in **Figure 6**.

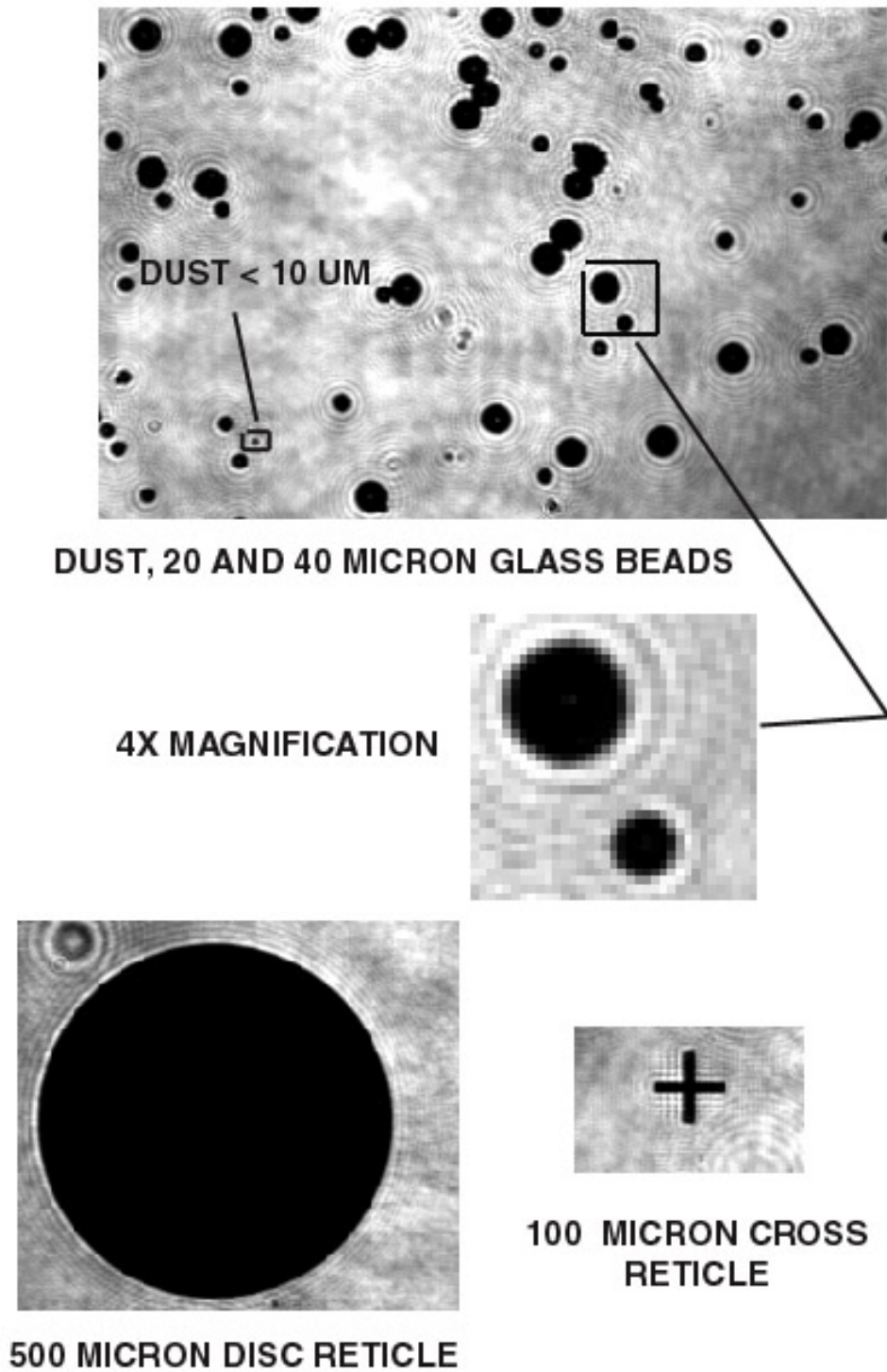


Figure 5. Images of glass beads, a cross reticle, and a large disc reticle taken with the prototype laboratory Micro-CPI optical imaging system.

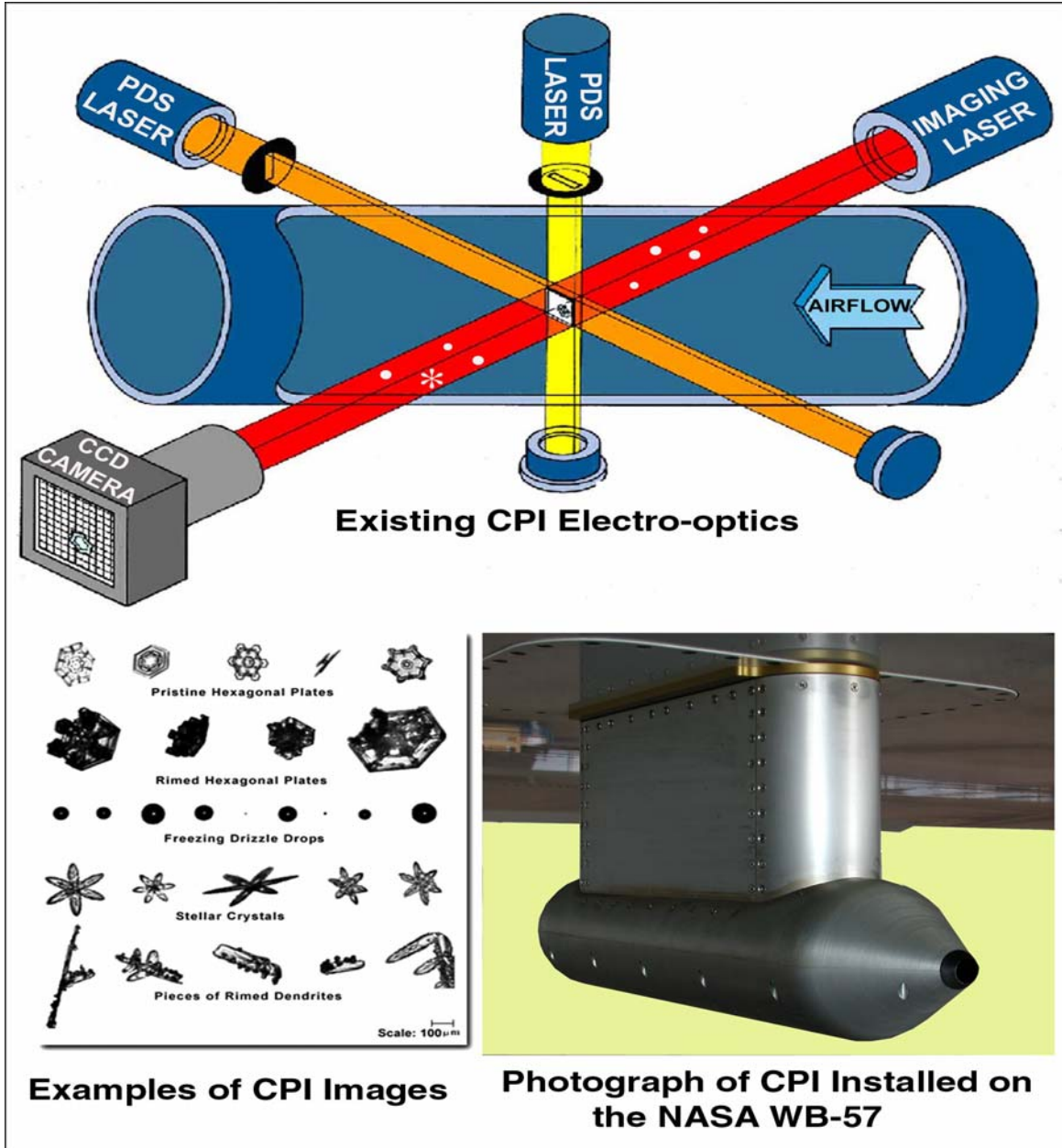


Figure 6. (Bottom Right) Photograph of the existing commercially available CPI installed on the NASA WB-57 aircraft, **(top)** schematic showing electro-optics and **(bottom left)** examples of ice crystal images. The Particle Detection System (PDS) in the existing CPI will be replaced by a Forward Scattering System (FSS) in the Micro-CPI that counts and sizes particles in addition to triggering the imaging system. Based on the images of glass beads taken in the laboratory (**Figure 5**), the Micro-CPI is expected to produce similar quality images of ice crystals.

2.3 Micro-CPI Image Throughput Analysis

One of the primary functions of the system electronics is to store the images of particles captured by the CMOS chip to memory. If the data rate is low enough, the entire full frame CMOS array image can be stored on each particle event. The data rate can be calculated by making some reasonable assumption on the number of particles passing through the sample volume. The forward scattering system used to trigger the imaging laser will have a sample volume of approximately 0.2 mm^2 . At flight speeds of 25 m s^{-1} , the resultant sample volume (S_{vol}) would be

$$\begin{aligned} S_{\text{vol}} &= 0.2 \text{ mm}^2 \times 25 \times 10^3 \text{ mm s}^{-1} \\ &= 5000 \text{ mm}^3 \text{ s}^{-1} \\ &= 5 \times 10^{-3} \text{ L s}^{-1}. \end{aligned}$$

For the sake of analysis, we assume a typical cloud drop concentration of 100 cm^{-3} ($100,000 \text{ drops L}^{-1}$), which leads to the theoretical particles per second detected (N_d) of:

$$\begin{aligned} N_d &= 5 \times 10^{-3} \text{ L s}^{-1} \times 100 \times 10^3 \text{ L}^{-1} \\ N_d &= 500 \text{ drops s}^{-1}. \end{aligned}$$

A maximum drop concentration, on the order of 10^6 , would yield an

$$\begin{aligned} N_d &= 5 \times 10^{-3} \text{ L sec}^{-1} \times 10^6 \text{ L}^{-1} \\ N_d &= 5 \times 10^3 \text{ drops s}^{-1}. \end{aligned}$$

The CMOS sensor is capable, when run in 640×480 image size (smaller than the 1280×1024 pixels for the whole chip), of 124 frames per second (fps). In single shot mode—the mode necessary for taking snap shot images of particles—this number is a little smaller, about 100 fps. At this rate, if no region of interest (ROI) selection were performed and the entire image were written to flash disk, a 2 GB disk would be filled in

$$2 \times 10^9 \text{ bytes} / (640 \times 480 \times 100 \text{ bytes s}^{-1}) = 65 \text{ s}.$$

Since an Aerosonde research flight will last much longer than 65 seconds, this is not acceptable. It is clear that particles or “regions of interest” (ROIs) must be cut out of the full frame image and individually stored to memory, and the rest of the image frame ignored. An algorithm to identify ROIs and save them to disk has been already been developed and is a mature technology in the commercially available aircraft CPI. However, this algorithm uses a dual-processor Pentium computer and our application will require that an algorithm be developed using both custom logic and the ADSP2191, the digital signal processor (DSP) that will control the Micro-CPI data acquisition system. The design for the Micro-CPI ROI algorithm is described in the next section.

2.4 Micro-CPI ROI Identification Algorithm

The CMOS array is read one row at a time. When no particle is present, a background image is stored. This is accomplished by flashing the image laser and recording the illuminated gray scale level for each pixel. During normal operating mode, when the image laser is flashed after being triggered by the FSS, as each pixel value in the row is read, a background value for the same pixel is compared via a logic circuit to determine if the imaged pixel is darker than the

background pixel. If the comparison is true for some number of pixels in a row, the pixel is considered a valid image pixel.

A preliminary logic design has been tested just to see if the first and last pixel can be found for each row by doing comparisons pixel by pixel at the clocked output rate of the CMOS sensor. The required DSP processing speed was analyzed assuming one particle per frame and a particle size of 20 x 20 pixels. Assuming each range calculation for determining N_{first} to N_{last} takes 10 instruction cycles, plus an extra 50 instruction cycles (a conservative number of cycles for the calculations that need performed) to calculate the range of bytes pixels⁻¹ for previous and subsequent rows, then the number of cycles spent doing calculations is:

$$10 \text{ cycles} \times (\text{image rows}) + 50 \text{ cycles} = (10 \times 20) + 50 = 250 \text{ cycles of overhead.}$$

The ADSP2191 runs at 160 MHz maximum, so it will perform these calculations in $250 / (160 \times 10^6) = 1.6 \mu\text{s}$. The data could then be written at 10 MB s^{-1} to the flash disk. So, to process such an image and store the data to flash memory would require $1.6 \mu\text{s} + (28 \times 28 \text{ bytes}) \times 10^{-6} = 785 \mu\text{s}$ (4 pixels to either side of the sensed particle will be recorded for best image processing, leading to 28 x 28 bytes rather than 20 x 20).

Even if the estimate on DSP processing were off by a factor of 100, the time to process and store the data to flash memory would be 944 μs . Rounding up to 1 ms, the system would be capable of processing and storing 1000 such particles per second: 10 times faster than the CMOS sensor can run. Up to 10 such particles per frame, at 100 fps (equaling 1,000 particles s⁻¹) can be recorded, which is more than adequate.

Assuming 2.9 $\mu\text{m} \times 2.9 \mu\text{m}$ pixels, the imaged area would be 1.85 mm x 1.4 mm (at 480 x 640 pixels). In the high concentration example given above, where there are 1 million particles L⁻¹, and thus 1 particle every mm, the number of particles imaged would be $2.6 \text{ mm}^2 \times 1 \text{ particle mm}^{-2} =$ roughly 2.6 particles per image. In this case, at 100 images taken per second, and assuming the 28 x 28 pixel image recorded, the flash memory would fill up in $2.6 \times 10^9 \text{ bytes} / (28 \times 28 \times 100 \text{ bytes s}^{-1}) = 33,163 \text{ s}$, or 9.2 hours. Since it is very rare to encounter such high particle concentrations for extended periods of time, a more reasonable maximum average particle concentration of 100,000 particles L⁻¹ yields a data storage duration of 92 hours, well past the endurance of the Aerosonde.

2.5 Micro-CPI Laser Power and Pulse Duration Requirements

The commercially available aircraft CPI uses a 70 W pulsed laser that is pulsed at 30 ns to freeze the image of particles traveling at 150 m s^{-1} . The driver for the 70 W laser and the laser itself are too large and draw too much power to be used in the Micro-CPI. However, since the Aerosonde flies at a much slower airspeed ($\sim 30 \text{ m s}^{-1}$), the duration of the laser pulse can be longer, reducing the power requirements of the laser. The response characteristics of the VCA1281 CMOS sensor chip were used to simulate the effects of image intensity and blur for particles traveling at 30 m s^{-1} . **Figure 7** shows (blue line) the output count (maximum is 255) for the VCA1281 versus exposure time using a 1 W laser. The green line in the plot is the distance a particle will travel at 30 m s^{-1} . The distance traveled corresponds to blurring effects, since the longer the laser is on, the further the particle will travel during the imaging period. ADC counts of roughly 100 should provide enough signal-to-noise to generate good images. An ADC value of 100 would correspond to a laser pulse width of approximately 0.13 μs and a blur

of approximately $3.5 \mu\text{m}$, or slightly more than 1 pixel. These estimates do not include the effects of laser power reflection losses in lenses, full width half maximum pulse times, etc., but experience with the CPI indicates less blur is expected. Spectra Physics manufactures a 1 W fiber coupled laser, model SFB100-808-V1-01, which will produce the results shown in **Figure 7** and is small and light enough for use in the Micro-CPI.

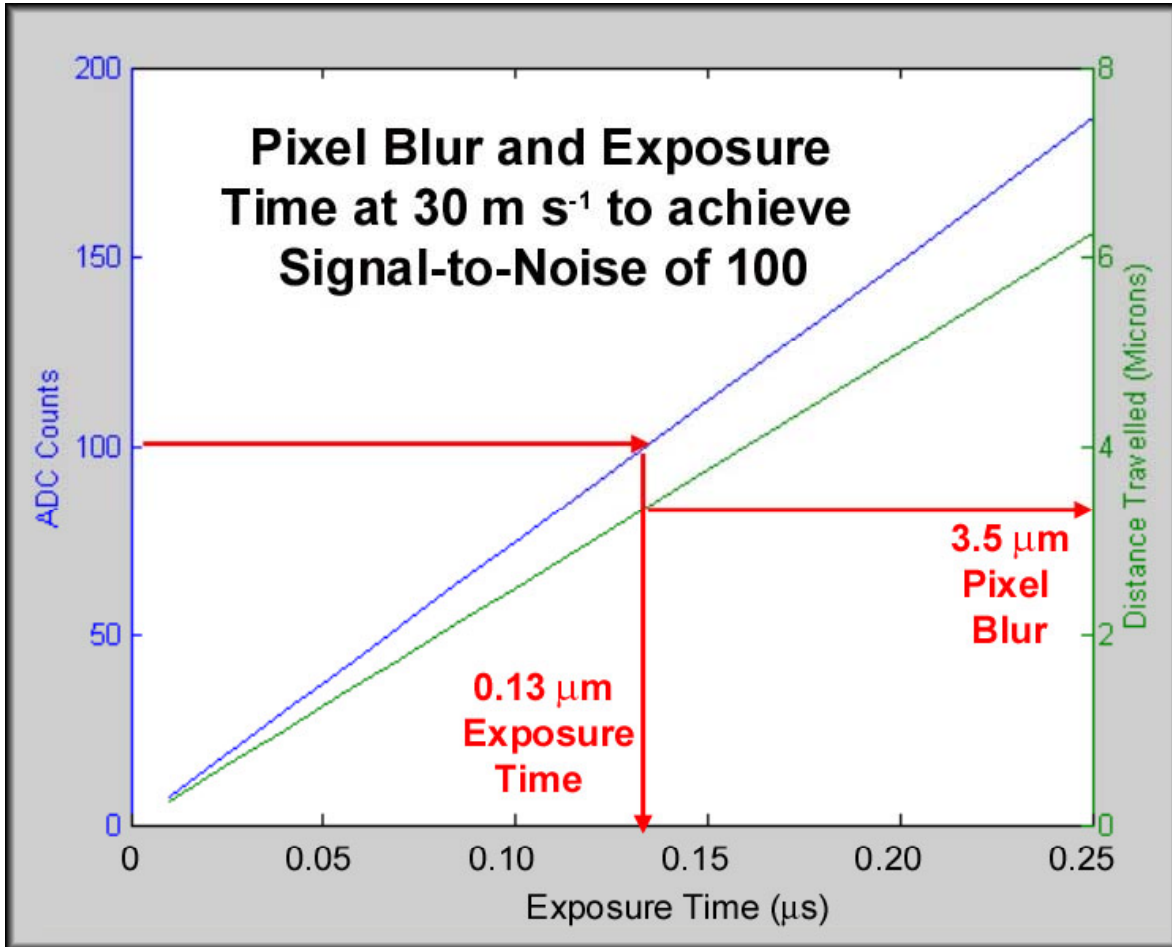


Figure 7. Plots showing (green line) that $3.5 \mu\text{m}$ of image blur (approximately 1 pixel) will occur for a $0.13 \mu\text{s}$ laser pulse to achieve a camera signal-to-noise of 100 (blue line) at an Aerosonde true airspeed of 30 m s^{-1} .

2.3 Imaging Optical Layout for Micro-CPI

Figure 8 is a ray trace of the system modeled in **Figure 3** with three folding mirrors added to change the overall dimensions of the optical layout. The optical path length, however, is identical to the system in **Figure 3**. The addition of folding mirrors will allow the imaging system to be packaged more effectively into the Aerosonde. Folding mirror 3 will be mounted directly to the CMOS array chip on the system electronics board. Details of the packaging are discussed in **Section 2.11**.

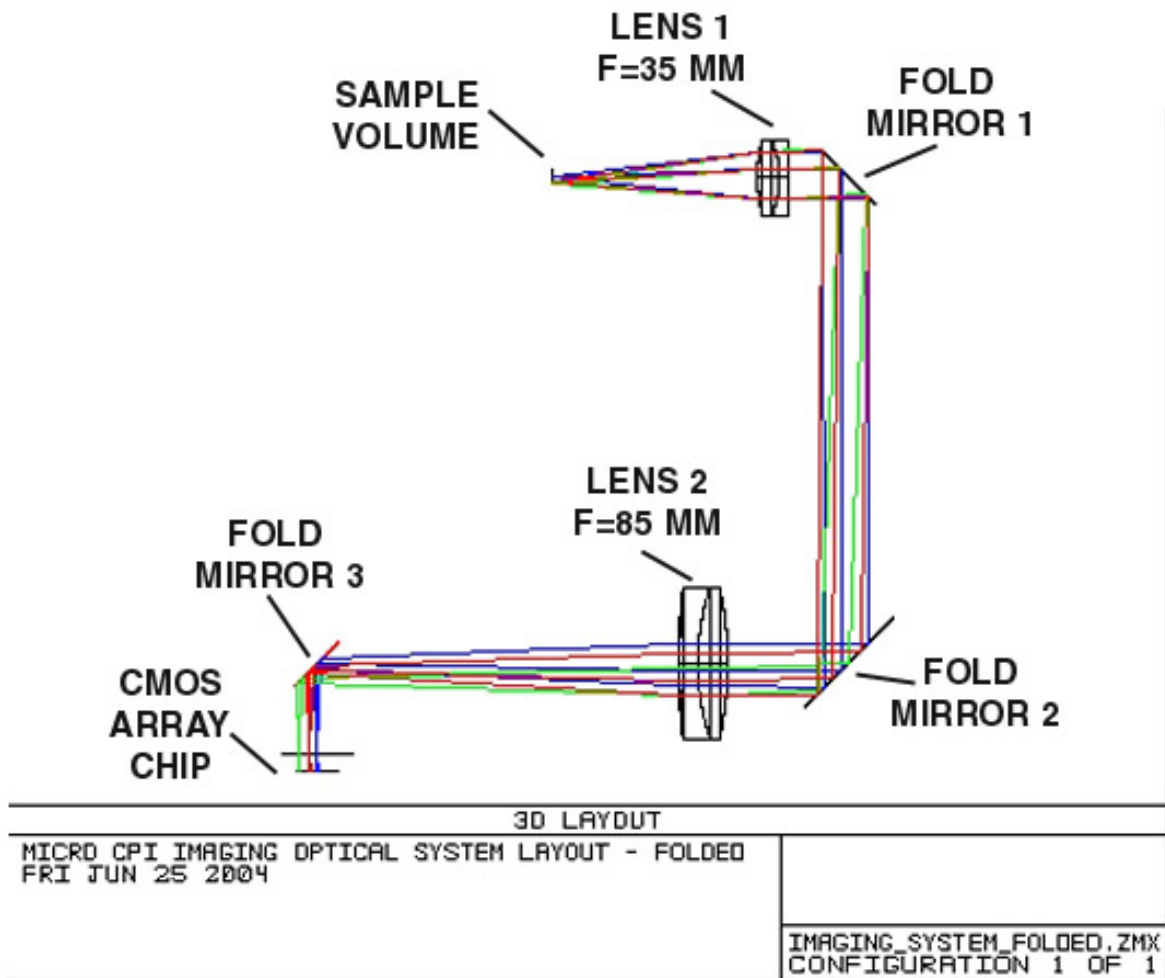


Figure 8. Ray trace showing imaging optical layout with the addition of three folding mirrors to minimize the size of the Micro-CPI.

2.7 Micro-CPI Forward Scattering System

A forward scattering system (FSS) will provide the dual functions of triggering the Micro-CPI imaging system and also provide independent particle sizing measurements that will operate continuously, even while the imaging system is busy downloading images from the CMOS camera. The basic layout for the forward scattering system is shown in **Figure 9**. A laser beam is used to uniformly illuminate the sample volume. The laser beam passes through the sample volume and intersects a prism where the beam is deflected to a power detector. When no particles are present, there is no scattered light present on the measured signal detector and qualifier signal detector. As a particle passes through the sample volume, light is scattered around the folding prism and onto the detectors. When the particle is located in the center of the sample volume, the intensity of the light hitting the signal detector is proportional to the size of the particle.

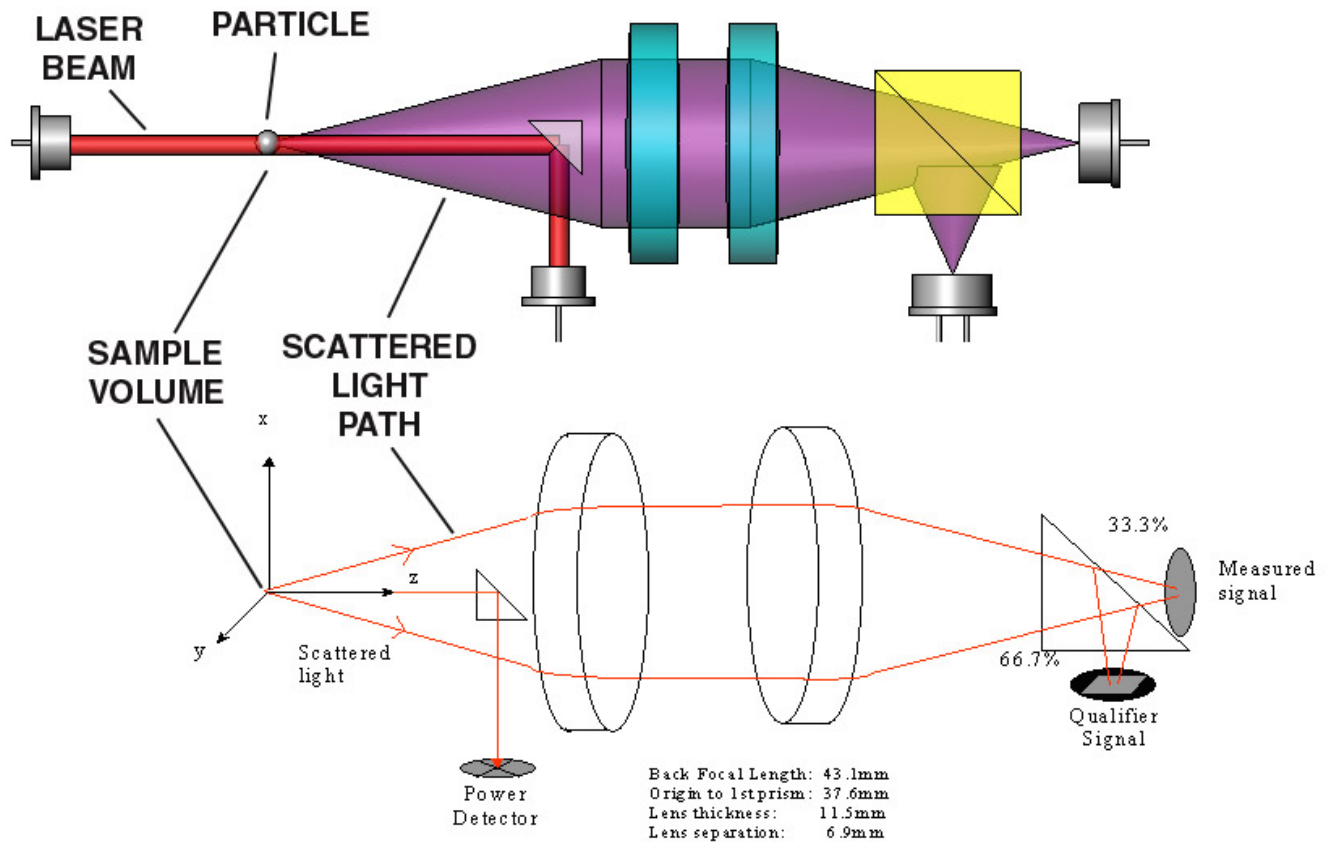


Figure 9. Schematic of the Forward Scattering System used to both trigger the imaging laser and provide continuous particle sizing data.

A method used to limit sample volume errors is shown in the lower part of **Figure 9**. A prism is used to split the scattered light, such that 33.3% is used for a measured signal, and 66.6% for a qualifier signal. The qualifier detector is covered with a rectangular slit aperture. The aperture only allows scattered light to reach this detector when a particle is near the center of the sample volume. If the particle falls within the sample volume, the qualifier signal will be larger than the measured signal, due to the prism transmission percentages.

As a particle moves out of the focal point in the $\pm z$ direction, the image size will increase, with several effects. First, the intensity of the scattered light ($W m^{-2}$) will decrease at the measured and qualifier detectors because the image becomes blurry. Second, the blurred image on the qualifier detector will, at some point, begin to fall outside the confines of the qualifier slit, causing the qualifier signal to decrease. When the qualifier signal falls below the measured signal the particle is rejected. This qualifier signal is used to define the sample volume and this technique is known as a depth of field rejection.

As a particle moves out of its focal point in the $\pm y$ direction, the effect is two-fold. First, the light collected is no longer symmetrically scattered; and second, the image begins to fall outside

the qualifier slit. Again, the particle will be rejected if the measured signal is greater than the qualifier signal.

Particles move through the sample volume in the + x direction. Because a particle will produce errors unless it is centered in the beam, as explained for $\pm y$ centering errors, the qualifier and measured detector signals are only measured at the maximum signal, a peak, seen at the signal processing electronics. Thus the sampling electronics ensure a particle is measured when centered in the x-axis.

Figure 10 shows the forward scattering cross section, in cm^2 , for water drops from below 1 μm diameter to 85 μm in diameter. The plot was generated assuming a 680 nm wavelength laser and a forward collection angle range of 5 to 12 degrees. The intensity of a particle's scattered light can be calculated from the scattering cross section times the laser beam intensity. Avalanche photodiodes (APD's) are used as detectors due to their fast response time and ability to detect low light levels. With a 10 mW laser producing an ellipse with major axis diameter of 1 mm and minor diameter axis of 0.5 mm, the APD current and signal to noise were analyzed for particle sizes from 2.5 μm to 100 μm , shown in **Figure 11**.

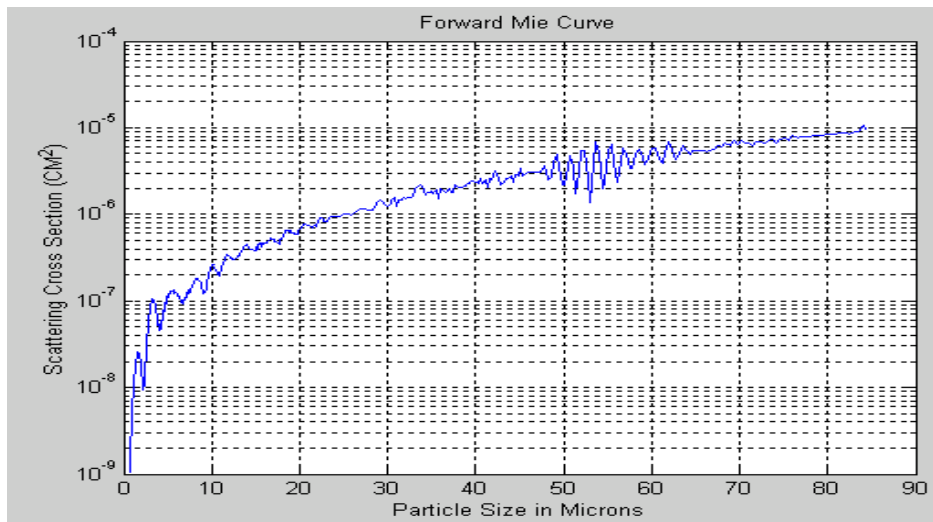


Figure 10. Forward scattering cross section versus particle size.

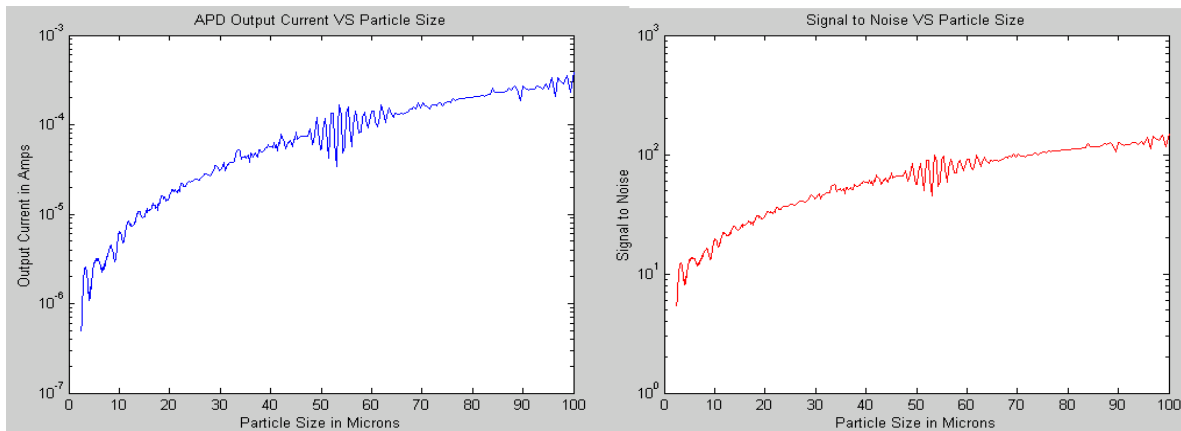


Figure 11. APD current and signal to noise versus particle size.

The plots in **Figure 11** begin with a 2.5 μm particle, and the lower limit of current and signal to noise just above that minimum size is 1 μA and 10, respectively. These values are acceptable limits, providing the ability to size particles over a size range of 2.5 μm to 100 μm .

To measure this current, a two-stage transimpedance amplifier system will be used, and the outputs of both stages fed to peak detect and threshold detect circuits, almost identical to the particle detection system used on SPEC's commercially available CPI. **Figure 12** shows the modified circuit for performing the necessary functions. Note that there are two nearly identical circuits, one for the sizing signal (upper half) and one for the qualifier signal (lower half). The circuit(s) perform the following functions:

- i.* Transimpedance amplification.
- ii.* Threshold detection.
- iii.* Peak detection (for sizing).
- iv.* Peak comparison (particle qualification).

The peak signal, labeled "SIG_PK" in the figure, will be sampled using an Analog Devices AD7671 analog to digital converter (ADC), which has also been used successfully in the commercially available CPI instrument. Each time a qualified, threshold detected particle event occurs, the peak value will be sampled and the particle is sized, as described in the following simulation.

Figure 13 shows signals from the circuit as they would be measured on an oscilloscope. V_SIG is the signal that feeds the threshold and peak detector circuits, as measured by the measured signal detector APD. V_QUAL also feeds threshold and peak detector circuits for the qualifying signal detector APD (refer to **Figure 9**, where the signal and qualifying detectors are shown receiving the scattered light). The two peak detectors produce SIG_PK and Q_PK, and Q_PK has the largest amplitude. This is the case when particles are within the depth of field sample area, and is indicated by the PTCL_GOOD signal going high.

The blue lines in **Figure 13** represent the threshold at which the control system electronics will recognize a particle event has occurred. Both the signal and qualifier will be monitored to ensure no particles outside the depth of field can get through and cause one or the other circuit's peak detectors to hold a peak that is later used incorrectly when a particle that is within the depth of field comes through.

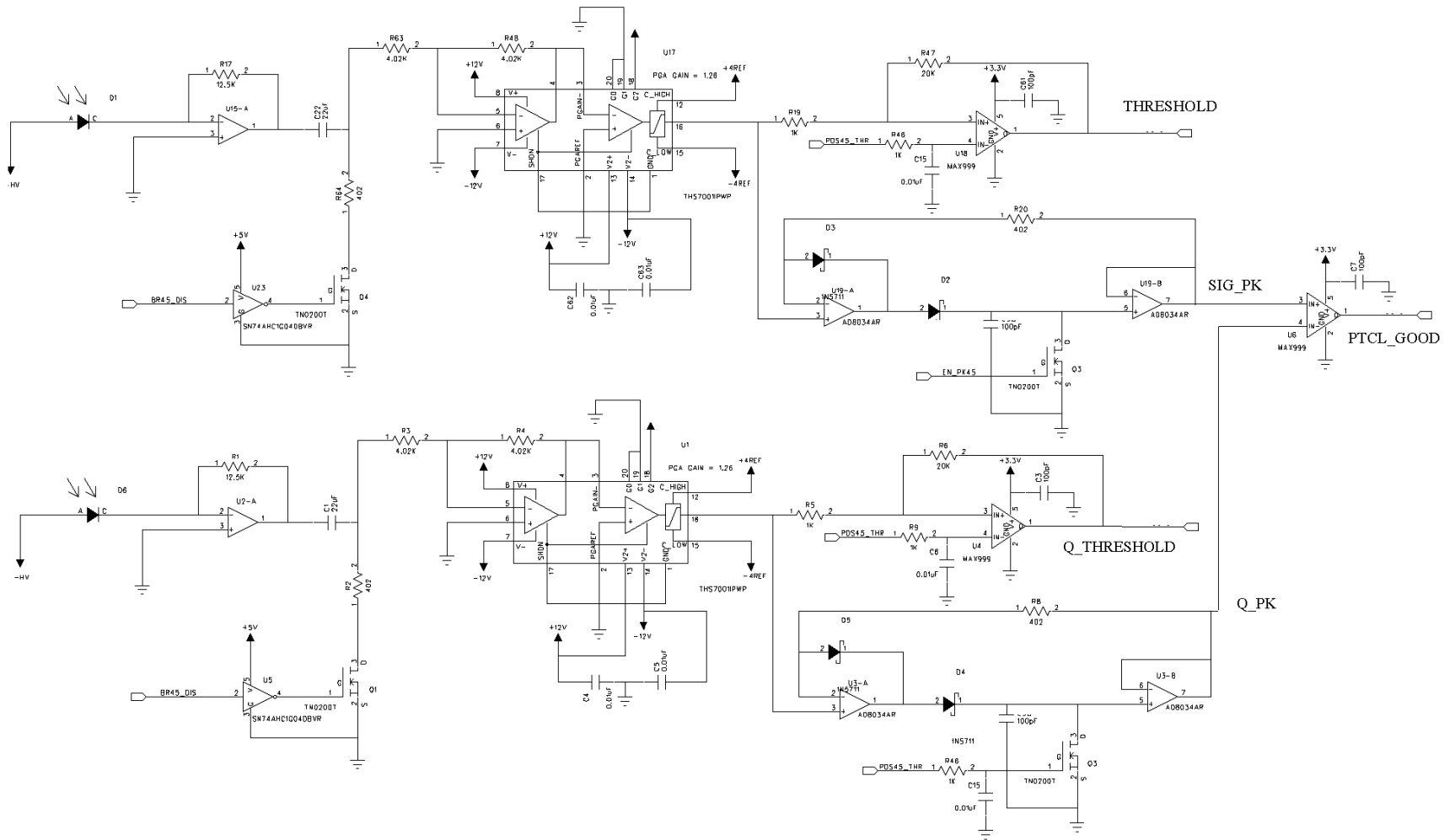
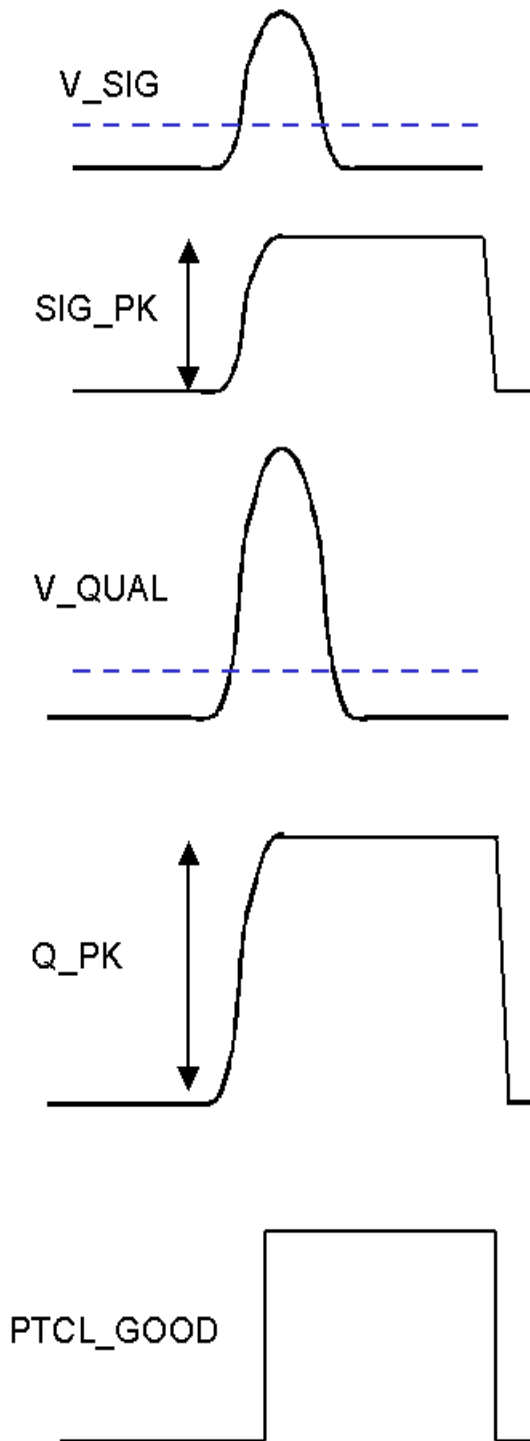


Figure 12. Electronics circuit for one gain stage of the forward scattering system.



Once both signals drop below the threshold (blue line) for a minimum period, the control electronics will check to see that the PTCL_GOOD signal is high. If it is, a sample of the SIG_PK signal will be taken for particle sizing; the peak detectors will then be cleared and the DC blocking capacitor charge will be shunted to ground via a transistor, preparing the circuit for the next incoming particle.

In the highest concentrations of 1 million particles L^{-1} , one could expect, at 25 m s^{-1} airspeed, to have 5,000 of these events per second (see **Section 2.3**). The circuit presented, with some adjustments to the high pass filter and charge shunt RC values ($C = 10\text{nF}$, $R_{sh} = 100 \text{ Ohms}$), can handle this concentration well, providing very good counting statistics for high particle concentration environments.

2.8 Layout for Micro-CPI Scattering System

The optical layout for the forward scattering system (FSS) to mount in the Aerosonde is shown in **Figure 14**. Two folding mirrors are used to fold the laser optical path and the collected light optical path. This geometry will facilitate mounting into the Micro-CPI instrument designed for the Aerosonde. All the optical components and detectors for the receiving optics will mount in a lens tube, making a self-contained unit.

Figure 13. Signals present in the circuit shown in **Figure 12**.

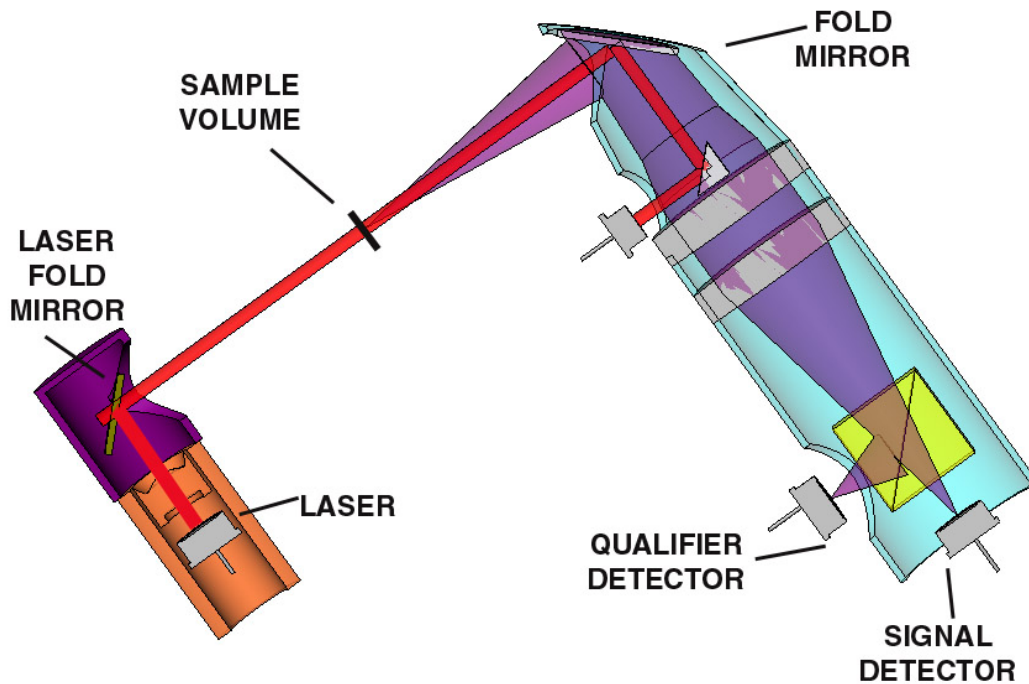


Figure 14. Layout for forward scattering system for Micro-CPI.

2.9 Micro-CPI Electronics System Design

Since gasoline is used to power the Aerosonde engine that drives the generator that produces electrical power, decreasing instrument power requirements increases flight duration. In order to mechanically integrate the proposed instrumentation into the Aerosonde payload, keep weight within limits, and operate at minimum power, a custom electronics system has been designed that integrates the forward scattering system (FSS) with the particle detection system used in the imaging system. A block diagram of the electronics board is shown in **Figure 15**. The major changes are integrating the two instruments, and using a CMOS sensor and a custom logic and microprocessor system, rather than a Pentium processor and frame grabber (or Firewire) based board. A further benefit of such a system, in addition to reduced electrical power and mass, is the reduced CPI system price. **Table 1** shows an estimate of costs of the major electrical components for the Micro-CPI.

Table 1. Price ranges for major electronics components of the Micro-CPI.

<i>Major Items</i>	<i>Highest Cost</i>	<i>Lowest Cost</i>
<i>CMOS Sensor</i>	<i>\$100</i>	<i>\$75</i>
<i>ADSP Processor</i>	<i>\$30</i>	<i>\$22</i>
<i>Logic CPLD</i>	<i>\$100</i>	<i>\$30</i>
<i>Flash Disk</i>	<i>\$450</i>	<i>\$75</i>
<i>PC Board</i>	<i>\$100</i>	<i>\$100</i>
<i>Total:</i>	<i>\$780</i>	<i>\$302</i>

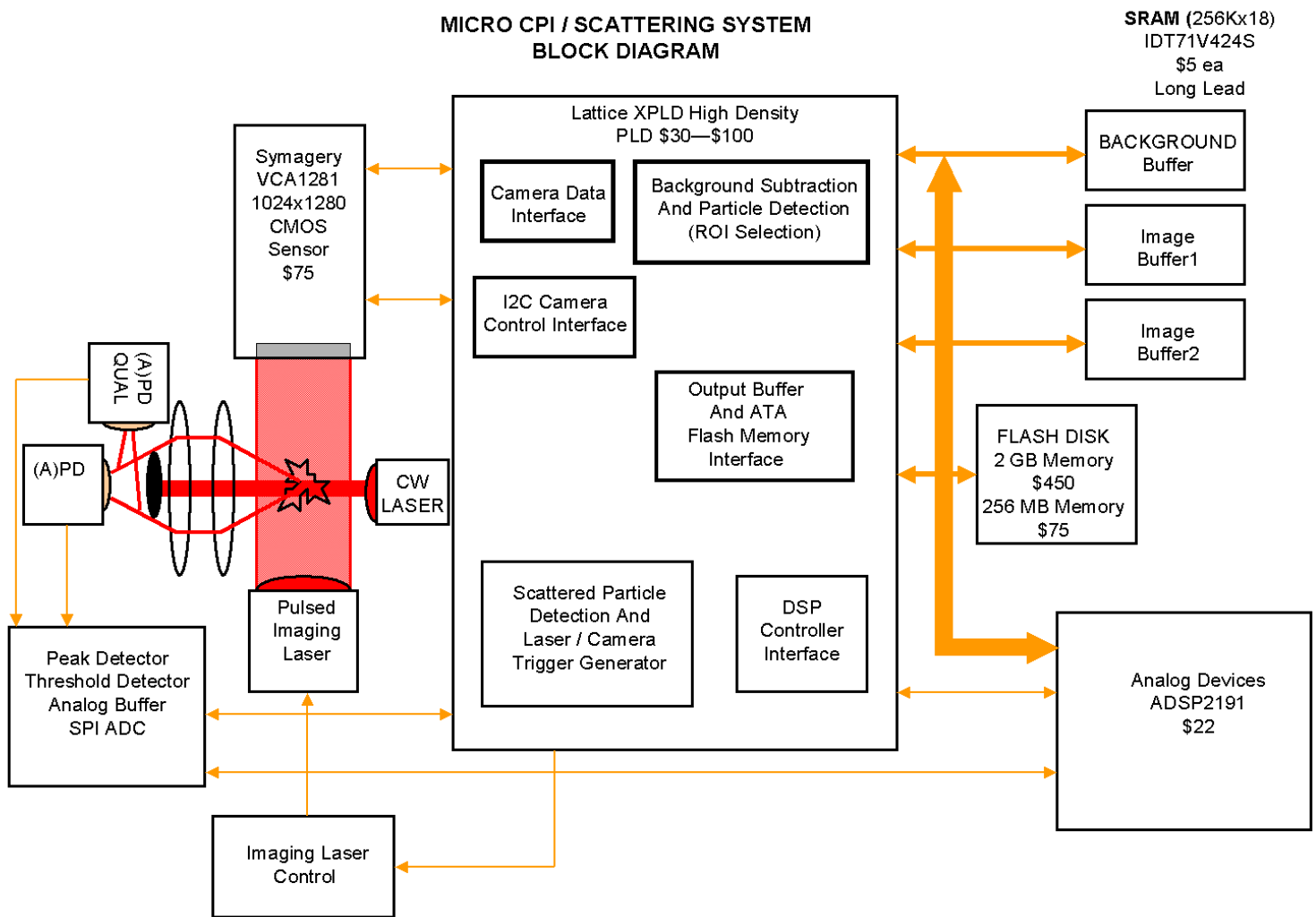


Figure 15. Micro-CPI electronics system block diagram

Contrast this price to that of the Scorpion camera alone (\$895), which is representative of full camera systems appropriate for the Micro-CPI, and the price benefit is immediately apparent.

2. 10 Micro-CPI Electronics Size, Mass and Power Budgets

The major components in the electronics system, as outlined in **Figure 15**, are given a sample placement in **Figure 16**. The board size is 3.75 inches x 4.5 inches x 0.5 inches—well within the Aerosonde payload bay dimensions—and is drawn with a 1:1 scale, as are the components.

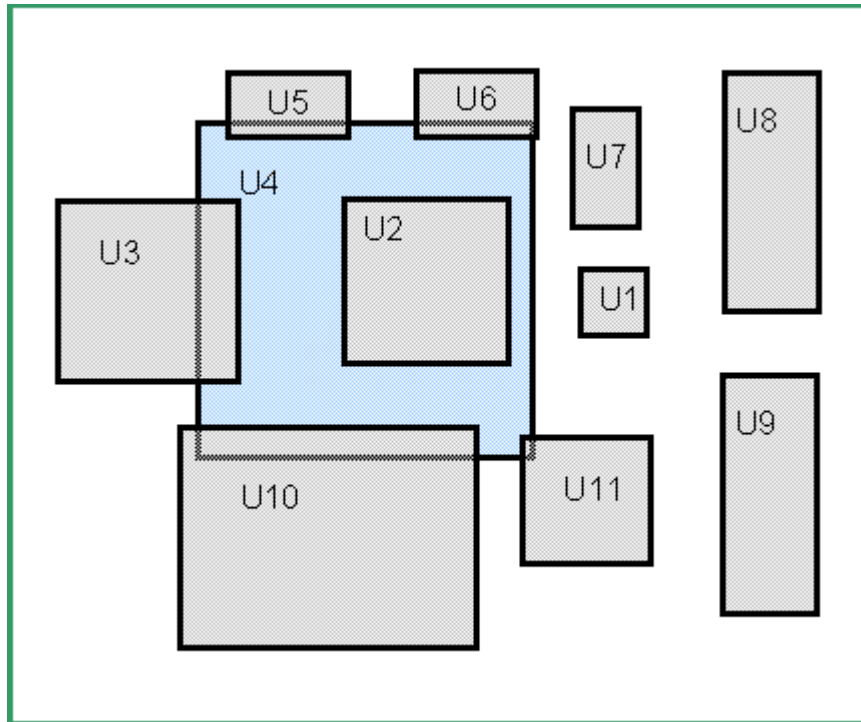


Figure 16. Sample component placement (1:1 scale) for electronics of **Figure 15.**

Table 2 shows the size, density, weight and power of the electrical components that comprise the Micro-CPI. The total weight is approximately 120 g and the total electrical power is 6.3 W. In the Phase I proposal, we estimated the Micro-CPI and scattering instrument would use 41 Watts and have a combined weight of 1620 grams, so the custom designs outlined here represent significant improvement. The remaining power in the Micro-CPI power budget allows some heating control capability that would allow the Micro-CPI to operate in colder environments, expanding its range of operating limits, while a majority of the weight budget is available for the mechanical and optical designs.

Table 2. Major electronic system component power and weight estimates.

Component Description	Size	Density (g in⁻³)	Weight (g)	Power (W)
U1: AD7671 ADC	0.354 x 0.354 x 0.063	22.5	0.18	0.125
U2: ADSP2191 DSP	0.866 x 0.866 x 0.07	22.5	1.18	1.15539
U3: VCA1281 CMOS SENSOR	0.95 x 0.95 x 0.085	40	3.07	1.7
U4: COMPACT FLASH	1.75 x 1.75 x 0.096	30	8.82	0.165
U5—U7:71V424 IDT SRAM	0.63 x 0.345 x 0.148	22.5	2.17	1.584
U8—U9: FS ELECTRONICS	1.25 x 0.5 x 0.07	22.5	1.97	0.25
U10: HIGH VOLTAGE SUPPLY	1.5 x 1.15 x 0.5	45	38.81	0.6
U11: 5768MV ispXPLD	0.67 x 0.67 x 0.082	22.5	0.83	0.66
4 APDs	0.071 cubic inches	45	9.59	0.0006
CIRCUIT BOARD	4.5 x 3.75 x 0.093	18.1	28.41	
IMAGING LASER	1.32 x 0.75 x 0.45	45	20.00	0.04
Total:			115 g	6.3 W

2.11 Micro-CPI Mechanical System Design

The overall mechanical layout for the Micro-CPI is shown in **Figure 17**. The sample volume is located at the overlap region of the imaging system and the forward scattering system (FSS). Both of the optical systems incorporate the folding mirrors discussed previously. One of the image folding mirrors is mounted on the CMOS sensor to direct the imaging path onto the chip. The folding mirrors, optics, and detectors for the FSS mount in a lens tube that allows the system components to be optically aligned, independent of the instrument. The FSS collection optics system is then installed in the instrument and registered to the sample volume. The same technique can be used to align the imaging system.

Figure 2 (shown in **Section 2.1**) is a solid model of the Micro-CPI mounted in the Aerosonde. Optical access for the sample volume is through the top of the fuselage. Two aerodynamic shaped pylons or “ears” protrude from the fuselage and encase the laser assemblies on the transmit side and the optical collection assemblies on the receive side. The sample volume is just upstream of the wing and vertically slightly above the top surface of the wing. The sample volume is located far enough forward of the propeller to minimize the airflow disturbance in the sample volume caused by the propeller. Other instruments have flown on the Aerosonde in this position such as an icing detector and a virtual impactor particle spectrometer.

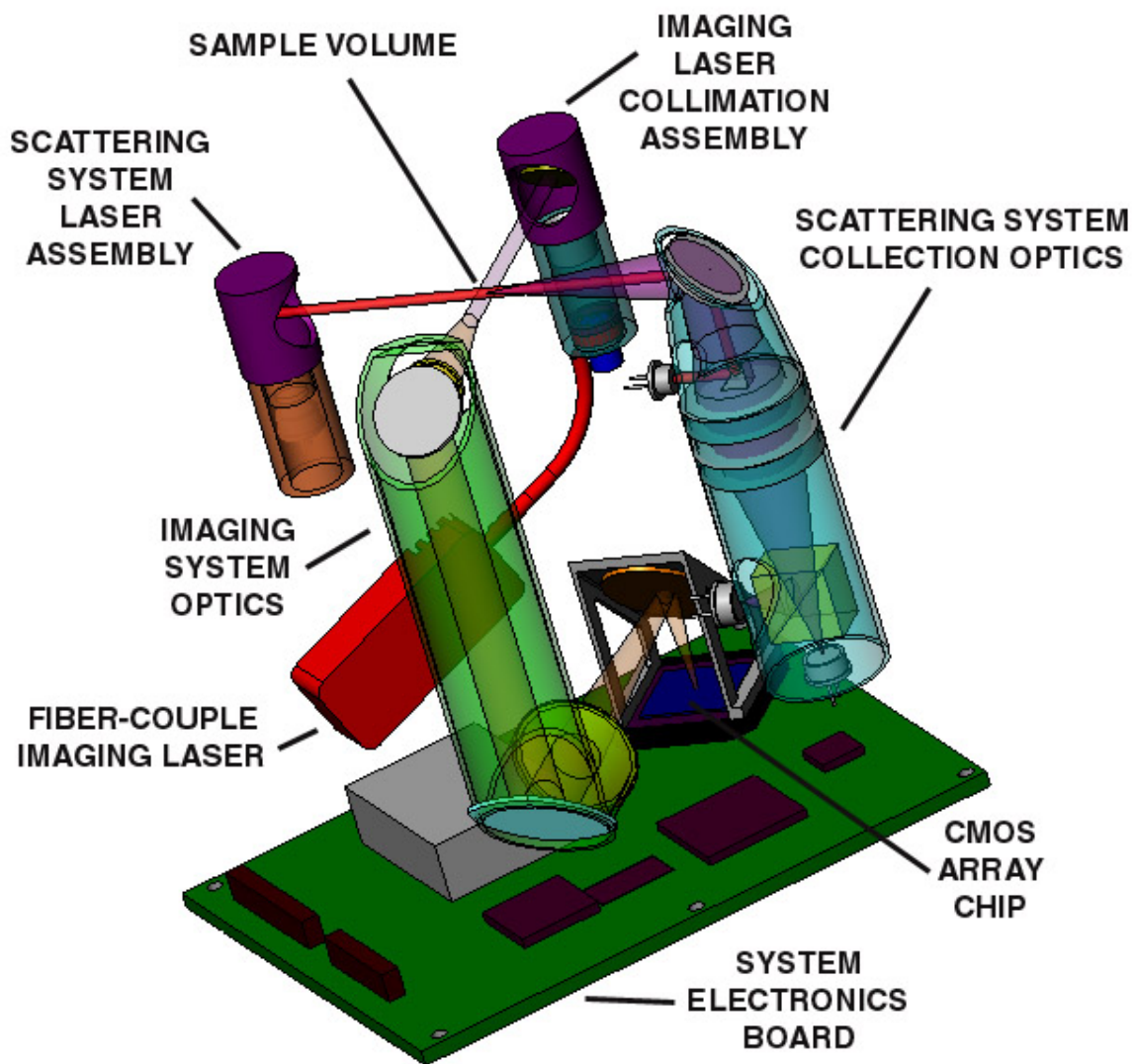


Figure 17. Solidworks solid model of Micro-CPI internal components.

A solid model of the complete Micro-CPI instrument is shown in **Figure 18**. A lightweight aluminum support structure and top mount plate are used as the primary structural support. The structural support mounts the lens tubes and laser assemblies in a fixed and registered position and mounts the system electronics board and CMOS chip assembly in a fixed and registered position to keep the imaging system in focus. Lightweight aluminum channel is used to mate the structural support to the Aerosonde payload bay. Vibration isolators are located at each corner of the structure to minimize the transmissibility of the vibrating aircraft engine to the Micro-CPI. The electrical interface connectors are located at the back end of the system circuit board.

Table 3 shows the component weights of the Micro-CPI mechanical and optical subsystems.

Table 3. Weights of Optical and Mechanical Components

Component	Mass (g)
<i>Optical access pylon</i>	120
<i>Optical support plate - top</i>	70
<i>Side support box</i>	140
<i>Lens tube - imaging system</i>	20
<i>Lens tube - scattering system</i>	16
<i>Imaging laser</i>	20
<i>Image laser barrel</i>	10
<i>Scattering laser barrel</i>	10
<i>Image system optics and mirrors</i>	50
<i>Scattering system optics and mirrors</i>	50
<i>Support base</i>	100
<i>Vibration isolation supports</i>	180
<i>Wiring and connectors</i>	100
<i>Fasteners</i>	100
<i>Miscellaneous Hardware</i>	100
TOTAL	1024 grams

The total weight of the mechanical and optical subsystems is approximately 1 kg. The instrument is mounted in the Aerosonde payload bay as far back toward the wing as is practical. This is to keep the instrument center of gravity near the wing surface to reduce the downward pitching moment on the aircraft. Most of the construction for the structural components of the instrument uses thin-wall aluminum. Other material possibilities will be investigated in Phase II, such as carbon fiber and other composite materials. However, the overall instrument weight of less than 2 kg may not warrant further effort. Flight duration considerations must be balanced with total instrument weight reduction efforts.

Since the Aerosonde uses a reciprocating engine, vibrations from the engine will be transferred through the airframe to the Micro-CPI. Vibration data for the aircraft have been obtained from Aerosonde and are shown in **Figure 19**. Vibration isolators will be used at each corner of the instrument mount structure to minimize the effect of the aircraft vibrations on instrument performance. **Figure 20** shows the response of a potential candidate vibration isolation system for the Micro-CPI. At frequencies greater than about 30 Hz, the Gel Bush B-1 isolator begins to damp out vibrations. The plot shown is for a total load of 10.5 kg. The Micro-CPI vibration isolator would require similar performance for a load of 1 – 2 kg.

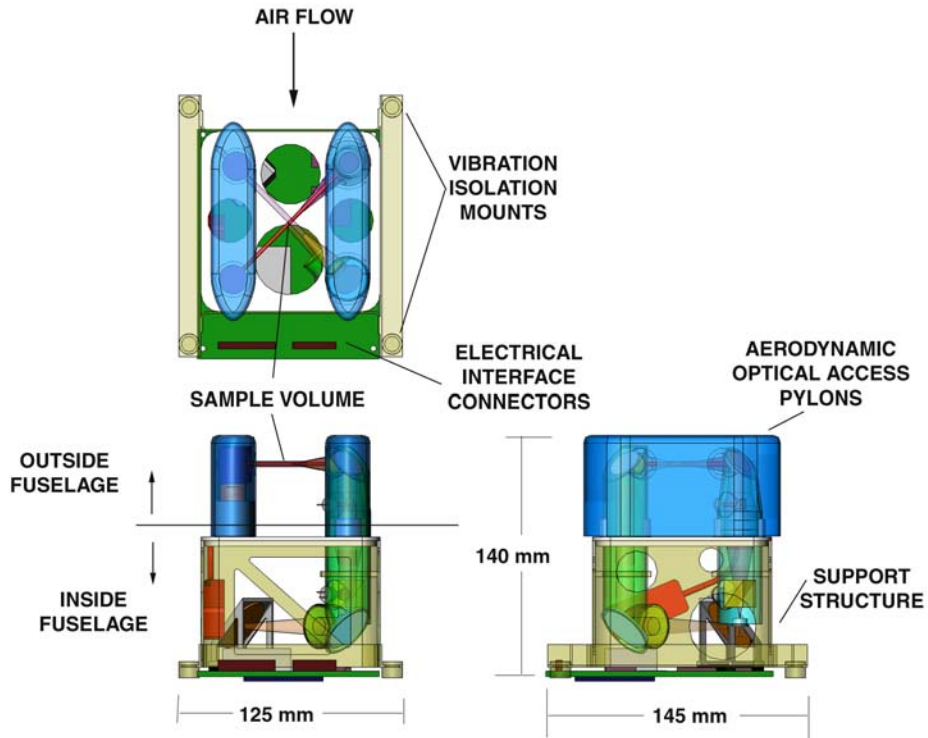


Figure 18: Packaging details of Micro-CPI

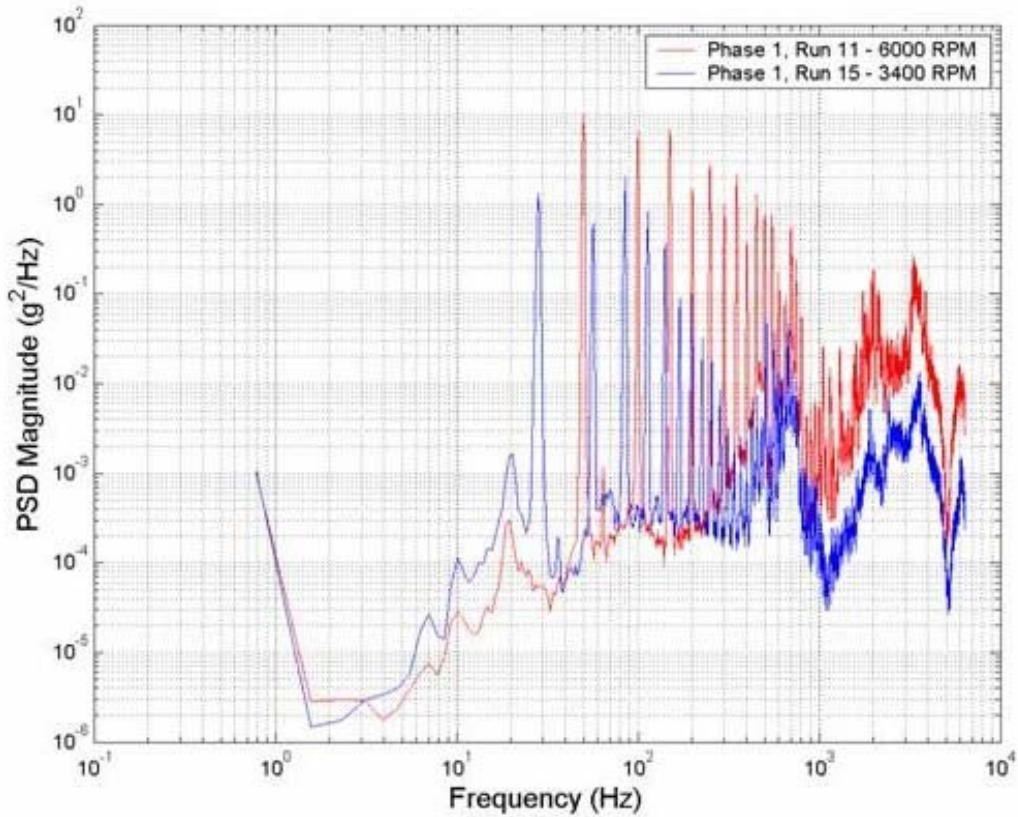


Figure 19. Vibration data for Aerosonde aircraft at two different engine speeds.

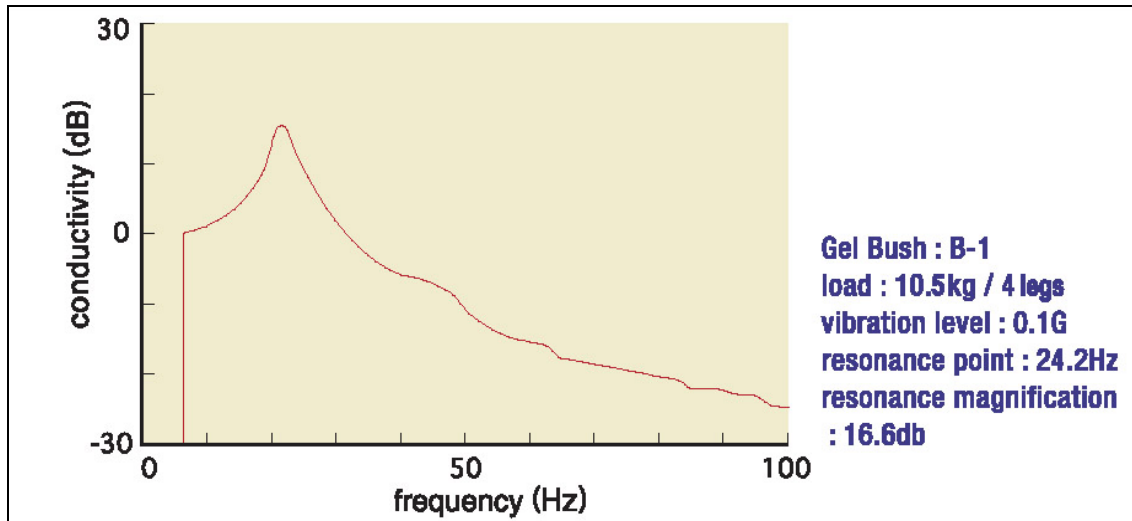


Figure 20. Frequency versus conductivity for potential vibration isolation system.

Table 4 summarizes the performance specification for the Micro-CPI instrument. SPEC has worked closely with the engineers from Aerosonde to design an instrument that is compatible for deployment on the Aerosonde aircraft. The size, weight, power, and sampling strategy are well suited for making cloud particle measurements from the Aerosonde.

Table 4. Final Micro-CPI Specifications

PARAMETER	VALUE	UNITS
<i>Sample area</i>	3 X 3.7	mm x mm
<i>Pixel resolution</i>	2.9	$\mu\text{m pixel}^{-1}$
<i>CMOS array size</i>	1024 x 1280 (480 x 640)	pixels x pixels
<i>CMOS array pixel size</i>	7	μm^2
<i>Max. Frame Rate</i>	30 at 1024 x 1024 (100 at 480 x 640)	frames per second at pixels x pixels
<i>Image system primary magnification</i>	2.4X	Linear magnification
<i>FSS beam diameter</i>	0.4	mm
<i>FSS collection angle</i>	5 - 12	Degrees
<i>Scattering system particle size range</i>	2.5 - 100	μm
<i>Total system electrical power</i>	6.5	W
<i>Total system weight</i>	1.144	kg

3. Phase II Technical Objectives

The objectives of the Phase II research are:

1. Refine Phase I analysis of Micro-CPI Forward Scattering System (FSS) and build breadboard FSS
2. Perform detailed design and fabrication of Micro-CPI system electronics board
3. Write software for instrument setup, download, and post-processing of data for Micro-CPI
4. Build integrated optical Micro-CPI breadboard
5. Perform detailed mechanical design, fabricate Revision A prototype Micro-CPI instrument, and test in laboratory
6. Install Micro-CPI onto Aerosonde aircraft and perform flight test series 1 at NASA Wallops Aerosonde Facility
7. Analyze data from Micro-CPI flight test series 1 and make modifications to instrument if required
8. Fabricate two Revision B prototype Micro-CPI instruments
9. Perform flight test series 2 at NASA Wallops Aerosonde Facility, analyze data, and write final report.

8. Subcontracts and Consultants

The Aerosonde Corporation (Aerosonde Pty Ltd of Melbourne, Australia) will be a subcontractor for the Phase II research. Aerosonde Corporation's task is described in the body of this proposal and the subcontract amount is shown in the Budget. Aerosonde is cost-sharing 50% of their labor costs. The availability of Aerosonde is confirmed in the Letter of Cooperation found in the Supplementary Documents Section of this proposal.

9. Potential Applications

The Micro-CPI developed under the proposed Phase II research will find myriad applications in both the research and operational communities. Research applications for the Micro-CPI will literally reach all regions of the globe. The Aerosonde has been used for atmospheric investigations ranging from polar regions to the tropics (visit www.aerosonde.com). The flight duration of the Aerosonde is 30 h and the ultimate research objective is to conduct long-term investigations of global weather conditions. The Aerosonde is relatively inexpensive (compared to research aircraft) and can be launched without a runway. Therefore, the potential exists for several hundreds or thousands of Aerosondes being equipped to measure cloud properties on a global scale. This establishes a very large market for the Micro-CPI.

Tethered balloons are now also being used to make long-duration measurements of cloud properties (Stamnes and Storvold 1999). The Micro-CPI could also find application on hundreds of tethered balloons. Both the Aerosonde and tethered balloons are proposed for the upcoming RIME project in Antarctica, expected to take place over the next 5 years.

In addition to the atmospheric science community, a relatively low-cost Micro-CPI could find several applications in industry. For example, several industrial processes, including the agricultural and painting industries, employ spray nozzles to distribute liquid product. These are huge industrial endeavors. The drop size distribution of these sprays directly impacts the efficiency of delivery. A low-cost sensor that provides a non-invasive measurement of drop-size distribution, such as the FSS probe proposed here, could represent an extremely large commercial market. Overall, the potential combined atmospheric research, operational atmospheric measurement and industrial markets for Micro-CPI cloud and spray applications is substantial.

A spin-off technology of the Micro-CPI Forward Scattering System (FSS) is the development of a very lightweight, low-power, low-cost standalone Micro aerosol and cloud probe for application on radiosondes. **Figure 23** shows a Solidworks model and a conceptual deployment on a radiosonde. As shown in **Table 5**, the Micro aerosol and cloud probe would measure particles in 30 size bins from 0.25 to 100 μm . Applications for the aerosol and cloud probe range from deployment in urban areas to regions of biomass burning and polar clouds.

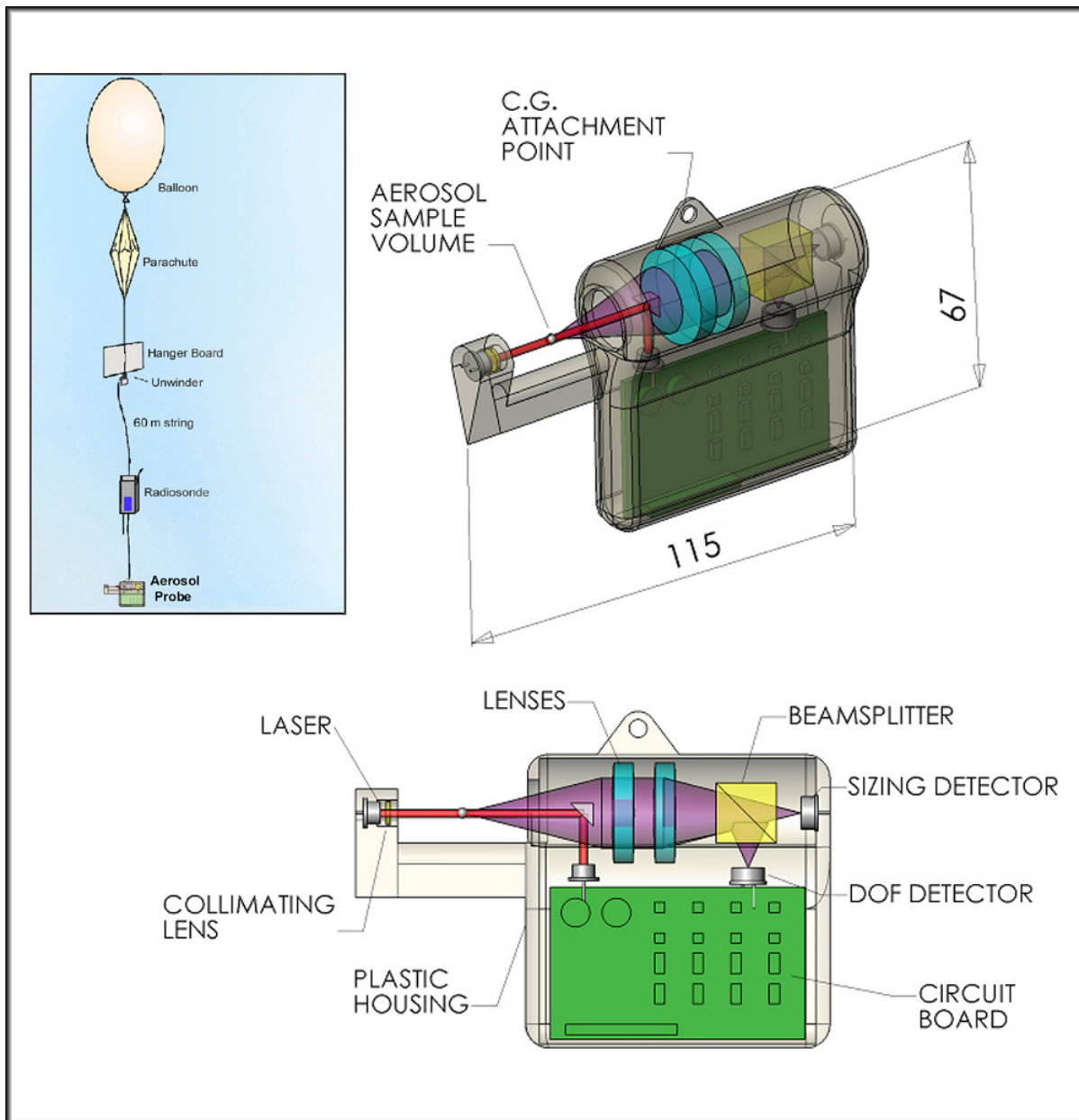


Figure 23. Solidworks models of a Micro aerosol and cloud probe and (inset) application on a standard weather (radiosonde) balloon.

Table 5. Specifications of the Micro aerosol and cloud probe

Weight	Power	Data Rate	Measured Parameters
160 grams (Electronics + Batteries)	4 Watts (1.5 hours operation)	30 channels plus 4 housekeeping (544 BPS)	Particle size 0.25um to 100um

Another possible commercial application for the aerosol and cloud probe is as a system to measure particulate matter in the atmosphere. The US Environmental Protection Agency (EPA) has revised rule 40 CFR 50 for ambient air quality surveillance regulations to include provisions for measuring particulate matter with an aerodynamic diameter less than or equal to 2.5 microns (PM2.5) (<http://www.epa.gov/fedrgstr/EPA-AIR/1997/July/Day-18/a18579.htm>). There are at least 1200 monitoring sites in the US that are part of the EPA PM2.5 monitoring network. For example, California has 81 PM2.5 monitoring stations that are part of the total EPA network (<http://www.arb.ca.gov/aqd/pm25/00final.pdf>). The Federal Reference Method (FRM) for measuring PM2.5 is to use an extractive technique with a special inlet with and an impactor that deposits the particulate matter less than 2.5 microns on a filter. The filter is then weighed at a laboratory after a sampling period of 24 hours and the mass of PM2.5 is calculated in micrograms per cubic meter. The Partisol Model 20000 air sampler available from Rupprecht and Patashnick is one of the FRM approved PM2.5 monitors of this type. This technique is very labor intensive and costly and results in only one PM2.5 measurement in a 24 hour-period. The PM2.5 level is reported 24 hours after it actually was collected in the atmosphere.

The aerosol and cloud probe can provide real-time measurements of the PM2.5 level with a measurement every few seconds. The measurement is in situ and does not require the expensive laboratory analysis to arrive at the measurement. The new scattering probe can be tested by the EPA and compared to the FRM for certification as a Class III equivalent method for PM2.5 measurement. The Micro-CPI scattering probe is much smaller and more portable than the Partisol 2000, which weighs approximately 70 lbs.

12. References

- Arnott, W. P., Y. Dong, and J. Hallett, 1994: Role of small ice crystals in radiative properties of cirrus: A case study, FIRE II, November 22, 1991. *J. Geophys. Res.*, **99**, 1371-1381.
- Baumgardner, D., H. Jonsson, W. Dawson, D. O'Connor and R. Newton, 2002: The cloud, aerosol and precipitation spectrometer (CAPS): A new instrument for cloud investigations, *Atmos. Res.*, **59-60**, 251 - 264.
- Cooper, W.A., and R.P. Lawson, 1984: Physical interpretation of results from the HIPLEX-1 Experiment. *J. Appl. Meteor.*, **23(4)**, 523-540.
- Fleishauer, R., V. Larson and T. Vonder Haar, 2001: Observed Microphysical Structure of Mid-Level, Mixed-Phase Clouds, *J. Atmos. Sci.*, **59**, 1779-1804
- Holland, G.J., P.J. Webster, J.A. Curry, G. Tyrell, D. Gauntlett, G. Brett, J. Becker, R. Hoag, and W. Vaglianti, 2001: The Aerosonde robotic aircraft: A new paradigm for environmental observations. *Bull. Amer. Met. Soc.*, **82 (5)**, 889-901. Download as PDF.
- Knollenberg, R.G., 1981: Techniques for probing cloud microstructure. *Clouds Their Formation, Optical Properties, and Effects*, P.V. Hobbs and A. Deepak, Eds., Academic Press, New York, NY. 15-91.
- Korolev, A.V., J.W. Strapp, G.A. Isaac and A.N. Nevzorov, 1998: The Nevzorov Airborne Hot-wire LWC-TWC Probe: Principle of operation and performance characteristics. *J. Atmos. Oceanic Technol.*, **15**, 6,1495-1510.
- Korolev, A.V., G.A. Isaac and J. Hallett, 1999: Ice particle habits in Arctic clouds. *Geophys. Res. Letters*, **26**, 9, 1299-1302.
- Lawson, R. P., 1979: A System for the Airborne Measurement of Vertical Air Velocity, *J. Appl. Meteor.*, **18**, 1363-1368.
- Lawson, R. P., 1980: On the Airborne Measurement of Vertical Air Velocity, *J. Appl. Meteor.*, **19**, 1416-1419.

- Lawson, R. P., and W. A. Cooper, 1990: Performance of some airborne thermometers in clouds. *J. Atmos. Oceanic Technol.*, **7**, 480-494.
- Lawson, R. P., and A. R. Rodi, 1992: A new airborne thermometer for atmospheric and cloud physics research. Part I. Design and preliminary flight tests. *J. Atmos. Oceanic Technol.*, **9**, 556-574.
- Lawson, R. P., R. E. Stewart, J. W. Strapp and G. A. Isaac, 1993: Aircraft observations of the origin and growth of very large snowflakes. *Geo. Res. Let.* **20**, 53-56.
- Lawson, R. P. and R. H. Cormack, 1995: Theoretical design and preliminary tests of two new particle spectrometers for cloud microphysics research. *Atmos. Res.*, **35**, 315-348.
- Lawson, R. P., and A. M. Blyth, 1998: A comparison of optical measurements of liquid water content and drop size distribution in adiabatic regions of Florida cumuli. *Atmos. Res.*, **47-48**, 671-690.
- Lawson, R. P., R. E. Stewart and L. J. Angus, 1998a: Observations and numerical simulations of the origin and development of very large snowflakes. *J. Atmos. Sciences*, **55**(21), 3209-3229.
- Lawson, R. P., A. V. Korolev, S. G. Cober, T. Huang, J. W. Strapp and G.A. Isaac, 1998b: Improved Measurements of the Drop Size Distribution of a Freezing Drizzle Event. *Atmos. Res.*, **47-48**, 181-191.
- Lawson, R. P., A. J. Heymsfield, S. M. Aulenbach and T. L. Jensen, 1998c: Shapes, sizes and light scattering properties of ice crystals in cirrus and a persistent contrail during SUCCESS. *Geo. Res. Let.*, **25**(9), 1331-1334.
- Lawson, R. P., L. J. Angus, A. J. Heymsfield, 1998d: Cloud particle measurements in thunderstorm anvils and possible weather threat to aviation. *J. of Aircraft*, **35**, 113-121.
- Lawson, R.P., B.A. Baker, C.G. Schmitt and T.L. Jensen, 2001: An overview of microphysical properties of Arctic clouds observed in May and July during FIRE.ACE. *J. Geophys. Res.*, **106**, 14,989-15,014.
- Miloshevich, L. M., and A. H. Heymsfield, 1997: A balloon-borne continuous cloud particle replicator for measuring vertical profiles of cloud microphysical properties: Instrument design, performance, and collection efficiency analysis, **14**, 753-768.
- Stamnes, K., and R. Stovold, 1999: Development and Deployment of a Powered Tethered Balloon System at the SHEBA Ice Camp for Measurements of Cloud Microphysical and Radiative Properties. Proceedings of the Ninth Atmospheric Radiation Measurement (ARM) Science Team Meeting, San Antonio, TX, March 22-26, 1999.
- Stith, J.L., J.E. Dye, A. Bansemer, A.J. Heymsfield, C.A. Grainger, W.A. Peterson and R. Cifelli, 2002: Microphysical Observations of Tropical Clouds, *J. Appl. Meteor.*, **41**, 97-117
- Weil, J. C., R. P. Lawson and A. R. Rodi, 1993: Relative dispersion of ice crystals in seeded cumuli. *J. Appl. Meteorol.*, **32**, 1055-1073.